PLOS ONE

RESEARCH ARTICLE

Digital spatial profiling of segmental outflow regions in trabecular meshwork reveals a role for ADAM15

Jennifer A. Faralli[1], Mark S. Filla[1], Yong-Feng Yang[2], Ying Ying Sun[2], Kassidy Johns[1], Kate E. Keller[2], Donna M. Peters[1,3]*

1 Departments of Pathology & Laboratory Medicine, University of Wisconsin, Madison, Wisconsin, United States of America, **2** Casey Eye Institute, Oregon Health & Science University, Portland, Oregon, United States of America, **3** Ophthalmology & Visual Sciences, University of Wisconsin, Madison, Wisconsin, United States of America

* dmpeter2@wisc.edu

OPEN ACCESS

Citation: Faralli JA, Filla MS, Yang Y-F, Sun YY, Johns K, Keller KE, et al. (2024) Digital spatial profiling of segmental outflow regions in trabecular meshwork reveals a role for ADAM15. PLoS ONE 19(2): e0298802. https://doi.org/10.1371/journal.pone.0298802

Editor: Paloma B. Liton, Duke University, UNITED STATES

Received: October 12, 2023

Accepted: January 30, 2024

Published: February 23, 2024

Peer Review History: PLOS recognizes the benefits of transparency in the peer review process; therefore, we enable the publication of all of the content of peer review and author responses alongside final, published articles. The editorial history of this article is available here: https://doi.org/10.1371/journal.pone.0298802

Data Availability Statement: All relevant data are within the manuscript and its Supporting information files.

Abstract

In this study we used a spatial transcriptomics approach to identify genes specifically associated with either high or low outflow regions in the trabecular meshwork (TM) that could potentially affect aqueous humor outflow in vivo. High and low outflow regions were identified and isolated from organ cultured human anterior segments perfused with fluorescently-labeled 200 nm FluoSpheres. The NanoString GeoMx Digital Spatial Profiler (DSP) platform was then used to identified genes in the paraffin embedded tissue sections from within those regions. These transcriptome analyses revealed that 16 genes were statistically upregulated in high outflow regions and 57 genes were statistically downregulated in high outflow regions when compared to low outflow regions. Gene ontology enrichment analysis indicated that the top three biological categories of these differentially expressed genes were ECM/cell adhesion, signal transduction, and transcription. The ECM/cell adhesion genes that showed the largest differential expression (Log2FC ±1.5) were *ADAM15*, *BGN*, *LDB3*, and *CRKL*. *ADAM15*, which is a metalloproteinase that can bind integrins, was upregulated in high outflow regions, while the proteoglycan *BGN* and two genes associated with integrin signaling (*LDB3*, and *CRKL)* were downregulated. Immunolabeling studies supported the differential expression of ADAM15 and showed that it was specifically upregulated in high outflow regions along the inner wall of Schlemm's canal and in the juxtacanalicular (JCT) region of the TM. In addition to these genes, the studies showed that genes for decorin, a small leucine-rich proteoglycan, and the α8 integrin subunit were enriched in high outflow regions. These studies identify several novel genes that could be involved in segmental outflow, thus demonstrating that digital spatial profiling could be a useful approach for understanding segmental flow through the TM. Furthermore, this study suggests that changes in the expression of genes involved in regulating the activity and/or organization of the ECM and integrins in the TM are likely to be key players in segmental outflow.

Funding: This study was supported by grants EY017006, EY032905 (DMP) and EY032590, EY019643 (KK) and Core grants P30 EY01665 (UW-Dept. of Ophthalmology) and P30 EY010572 (Dept. of Ophthalmology and Casey Eye Institute).

Competing interests: The authors have declared that no competing interests exist.

Introduction

Intraocular pressure (IOP) is maintained by the balance between the level of aqueous humor produced by the ciliary body and the rate by which it exits the eye through the trabecular meshwork (TM) in the anterior portion of the eye [1–4]. The movement of aqueous humor outflow is considered to be segmental, or non-uniform, around the circumference of the eye so that regions of high flow are intermingled with regions of low and medium flow [5–8].

What controls segmental outflow, however, remains to be determined. Regions of low and high outflow in the TM appear to be morphologically similar, although some differences have been noted that could explain segmental outflow. Regions of high outflow have been reported to be associated with collector channel ostia and distal vasculature [9, 10]. These high outflow regions often have a thicker, expanded TM [11] and contain fewer connections between the cells lining the inner wall of Schlemm's canal (SC) and the underlying JCT. More basal openings below giant vacuoles [12] have also been observed in high outflow areas. Interestingly, the distribution of these regions appears to be dynamic and age-dependent with older eyes exhibiting a slower redistribution then younger eyes [13, 14].

At the cellular level, both the composition of the extracellular matrix (ECM) and the cells residing in the JCT and underneath the adjoining inner wall endothelium of SC are thought to contribute to the movement of aqueous humor outflow across the TM [15–19]. Studies using transgenic mouse models and cultured anterior segments have indicated that changes in the expression of a variety of ECM proteins, including fibronectin [20, 21], collagens [22], SPARC [23, 24], thrombospondins [25], decorin [26], and myocilin [27, 28], affect outflow. ECM PCR arrays and proteomic studies further supported this idea and suggested that expression of some ECM genes and proteins, such as versican, VCAM, and TIMP1, appear to be enriched in certain regions of the TM relative to outflow [29–32].

Studies using cultured models of anterior segments have also shown that the biomechanical properties of the low and high outflow regions differ [30] and that low outflow regions appear to be regions where the tissue is stiffer. Subsequent proteomic studies on these tissues have found that significant differences in ECM proteins existed when the anterior segments were perfused at a higher pressure [30]. Among the proteins identified were several proteoglycans (keratocan, decorin, and lumican) that play a role in collagen fibril formation and the ECM proteins, dermatopontin and thrombospondin-4. Transforming growth factor β1 (TGFβ1) and MAM Domain Containing 2 (MAMDC2) were also identified in this study. Subsequent studies using TM cells isolated from these high and low outflow regions have also identified differences in the ECM proteins expressed by these cells but only after a prolonged time in culture [33]. Studies have also shown that variations in TM cellularity in high and low outflow regions do exist, but these differences did not appear to be correlated with segmental outflow [34]. Although the molecular differences identified in these segmental areas are likely to be correlated with differential outflow facility across different areas of the TM circumference [35], the molecular mechanism(s) that control normal aqueous humor outflow are still poorly understood.

In this study, we used digital spatial profiling of the transcriptomes of high and low outflow regions of human anterior segments to determine if differential expression of ECM or cell adhesion genes can account for segmental outflow. This study shows that relatively few structural ECM and integrin genes, with the exception of *DCN* and the *ITGA8* integrin subunit, showed any differential expression between low and high outflow regions. Rather, the changes observed were mainly in genes such as *ADAM15*, *CRKL*, and *LDB3* that regulate cell adhesion, especially adhesion involving integrins and most of the changes were less than 3-fold. This suggests that large changes in gene expression may not be involved in segmental outflow and that

outflow could be regulated by small changes in gene expression that control the activity of the ECM and cell adhesion molecules.

Materials and methods

Donor eyes

Normal human cadaver eyes were obtained from 3 males (ages 65–70). One male was Caucasian. The race of the other two donors was unknown. All eyes were acquired from Lions-Vision Gift, Portland, OR, and none of the eyes had a history of ocular disease. All studies were approved by the Oregon Health and Science University Institutional Review Board and were done in accordance with the tenets of the Declaration of Helsinki for the use of human cadaver tissue.

Anterior segment perfusion culture

Human cadaver eye globes (n = 3) were bisected and the lens, ciliary body, and iris were removed leaving the cornea, TM, and a small rim of sclera. Anterior segments from each donor eye then were placed in stationary organ culture as previously described [36]. Length of time from death to stationary culture was less than 48 hours and anterior segments were initially placed into serum-free stationary organ culture for 5–7 days to facilitate postmortem recovery. Anterior segments were then perfused with serum-free Dulbecco's Modified Eagle's Medium (a 1:1 mixture of high and low glucose DMEM) containing 1% Penicillin/Streptomycin/Fungizone until a stable baseline was achieved. Perfusion was done at a constant pressure (8.8 mmHg) with an average flow rate of approximately 1–7 μl/min, which is similar to normal physiological rate and pressures (minus episcleral venous pressure) in vivo [13, 30, 31, 33, 37].

Regions of segmental outflow were then determined by perfusing anterior segments for 1 hour with fluorescently-labeled amine-modified 200 nm FluoSpheres as described previously [31]. The distribution of fluorescently tagged FluoSpheres was imaged by fluorescence microscopy and wedges of anterior segments containing regions of high fluorescence intensity were dissected away from regions of medium and low fluorescence intensity (Fig 1A). Anterior segment tissue wedges containing the TM from high, medium and low outflow regions were then fixed with 4% paraformaldehyde in PBS for 30 min at room temperature. Tissues were then placed in 70% ethanol, shipped to University of Wisconsin (UW), and embedded into paraffin at the UW-Translational Research Initiatives in Pathology histopathology core facility.

NanoString digital spatial profiling (DSP)

Wedges of anterior segments from low and high outflow regions were prepared for DSP analysis as they would be expected to show the biggest differences in gene expression. Briefly, paraformaldehyde-fixed paraffin sections (5 μm) from the designated high and low outflow regions from the three eyes were cut, placed on a single SuperFrost Plus slide, and deparaffinized by baking the sections for 10 min at 60˚C followed by two 5 min xylene washes, a graded series of ethanol washes (100–50%), one 5 min nuclease-free water wash and two 5 min PBS washes. Antigen retrieval was performed by incubating the sections for 15 min at room temperature in 10 mM EDTA with 0.1 M Tris buffer (EDTA/Tris) at pH 9.0 (Invitrogen 00-4956-58) and then incubating the sections in 95˚C EDTA/Tris buffer for 20 min. Sections were allowed to gradually cool to room temperature for 20 min and then washed with two 5 min washes of TBS-0.05% Tween-20, pH 7.4. Sections were then incubated for 15 min at 37˚C with 1μg/ml proteinase K in PBS and then washed with PBS. This was followed by one 5 min wash with 10% neutral buffered formalin, two 5 min washes with NBF stop buffer and one wash with PBS.

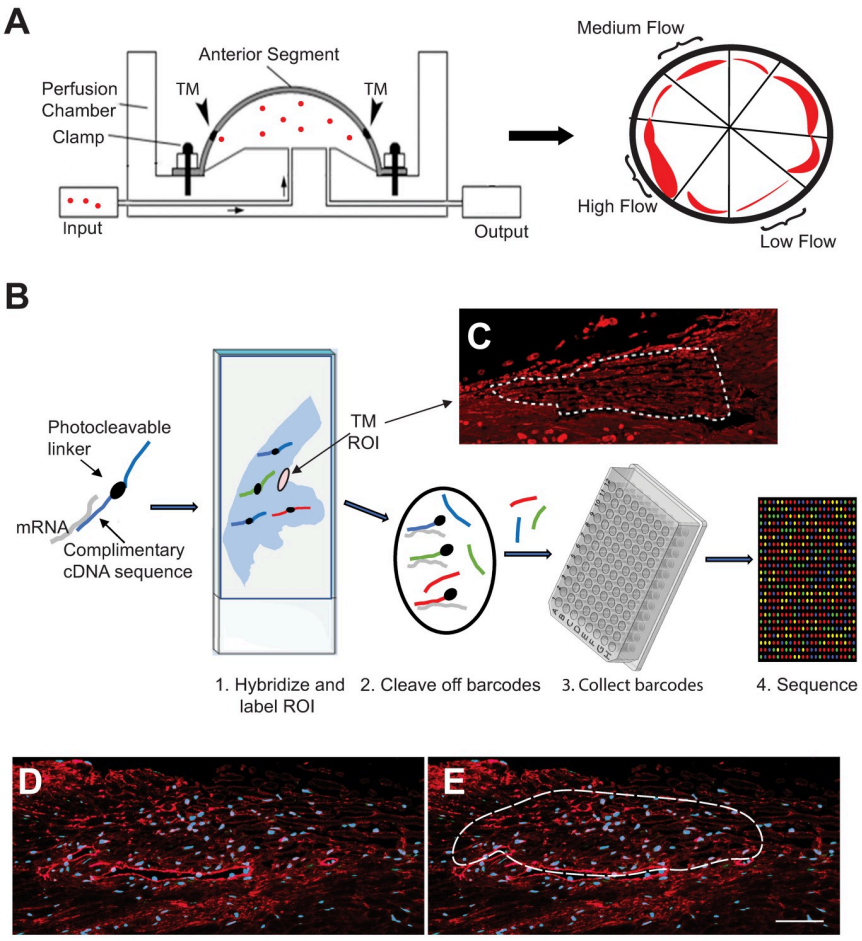

Fig 1. Schematic of the workflow for the study. (A) Schematic of organ culture system. Fluorescent beads (red dots) are perfused through a human anterior segment in organ culture. After 1 hour the anterior segment is divided into low, medium and high outflow regions based on the intensity of the fluorescent beads (red regions). (B) Images show steps in the DSP process. Tissue sections on a slide were labeled with DSP probes and ROIs were selected based on tissue morphology and fibronectin immunostaining. Barcodes in ROIs were cleaved using UV light and collected into a 96-well plate for sequencing. (C) Actual scan of fibronectin labeled tissue from a high outflow region with the ROI drawn. (D-E) Images of fibronectin (red) labeled tissue sections. Dashed line in panel E shows a typical size and location of the ROI used for the study. Nuclei (blue) were labeled with Hoechst 33342.

https://doi.org/10.1371/journal.pone.0298802.g001

Sections were then hybridized overnight with the GeoMx Human Whole Transcriptome Atlas (WTA) oligonucleotide probe mix (NanoString Technologies, Inc) according to the manufacturer's instructions. Each RNA probe was coupled with a unique photo-cleavable oligonucleotide barcode (Fig 1B). The tissue was then double-labeled with an anti-fibronectin antibody conjugated to Alex 647 (1:200 dilution Abcam 198934) and Syto13 (1:10 dilution Thermo NanoString GeoMx Nuclear Stain Morphology Kit 121300303). Labeled slides were imaged on the GeoMx® digital spatial profiler and the TM was identified visually by its unique morphological structure and the fluorescent labeling pattern of fibronectin. For each TM identified, a single polygon-shaped region of interest (ROI) ranging in size from 14,000–40,000 μm^2 was drawn around the TM encompassing the inner wall (IW) of SC, the JCT and the trabecular beams (Fig 1C). Each ROI was then illuminated with a UV light so the oligonucleotides probe barcodes present within each TM were photocleaved and collected individually into a single well of a 96-well collection plate. Barcodes were sequenced at the UW

Biotechnology Center on an Illumina NovaSeq 6000 and FASTQ files were then processed by the NanoString pipeline. Statistical analysis of the data was performed using a linear mixed model and the Benjamini-Hochberg correction factor to control for false discovery rate. Digital counts were normalized with internal controls for system variation.

Immunohistochemistry of high and low flow regions

Five-micrometer paraffin sections from high and low outflow wedges mounted onto glass slides were deparaffinized in xylenes followed by rehydration in a series of 100–50% ethanol solutions. Antigen retrieval was performed at 95˚C in 10 mM EDTA with 0.1 M Tris buffer at pH 9.0 for 20 min. The sections were allowed to cool to room temperature and were blocked for 1 hour with 1% BSA in PBS. Sections were then labeled with rabbit monoclonal anti-ADAM15 antibody (Abcam ab124698) diluted 1/800 in 1% BSA in PBS overnight at 4˚C. Sections were then washed with PBS and labeled with a secondary Alexa 546-conjugated goat anti-rabbit IgG (A11035; ThermoFisher Scientific) diluted 1/500 in the 1% BSA/PBS buffer. Nuclei were labeled with Hoechst 33342. Sections were washed with PBS and mounted with a glass coverslip using Shandon™ Immu-mount (ThermoFisher Scientific). Labeled cells were imaged using a Zeiss Imager.M2 fluorescence microscope together with Zen image acquisition software ver 3.079. Images of ADAM15 labeling were equally thresholded using Image J (National Institutes of Health) and the integrated density was calculated for the JCT and IW combined, the outer wall (OW) and beams of each image. High outflow (n = 11 wedges from 3 OD eyes) and low outflow (n = 9 wedges from 3 OD eyes) regions were averaged and statistical analysis was performed using ANOVA in conjunction with Tukey's HSD test.

Results

To get a better idea of how outflow facility may be regulated at the gene level, we used the NanoString GeoMx platform (Fig 1B) to compare the transcriptome of high and low outflow regions. The TM from 10 regions of high outflow and 13 regions of low outflow were selected as described in Materials and Methods. Not surprisingly, the transcriptomes of the two regions were very similar and only 74 genes were found to be statistically different ($p<0.05$). The majority of these genes (57 genes) were downregulated in high outflow regions compared to the low outflow regions and 16 genes were upregulated in the high outflow regions compared to low outflow regions (Fig 2). Somewhat surprisingly, only 10 genes showed a log2FC of ±1.5 or greater suggesting that large differences in gene expression were not associated with segmental outflow in the TM.

To identify biological processes that may be affected by the genes that were statistically different, gene ontology analysis was performed. Fig 3 shows that the biological classification involving the greatest number of genes which were differentially expressed between high and low outflow regions was associated with the ECM and cell adhesion. As shown in Table 1, most of the genes appeared to regulate cell adhesion or ECM organization and, with the exception of *ADAM15*, were all downregulated in high outflow regions. The greatest differences appeared to involve the genes *CRKL* and *LDB3* which encode for proteins found in focal adhesions that would affect integrin signaling. Both *LDB3* and *CRKL* showed a log2FC = -1.6 (or a 0.3-fold decrease) in expression. The next most downregulated gene was *BGN* (log2FC = -1.4), which showed a 0.4-fold decrease in expression. *ADAM15* (log2FC = 0.7), the only gene upregulated in the high outflow region, showed a 1.6-fold increase in expression.

Fig 4 shows the boxplots for the distribution of the *ADAM15*, *LDB3*, *CRKL* and *BGN* in high and low outflow regions of the TM. The majority of the values for each of these genes fell within the interquartile range (IQR, Q1-Q3) indicated by the box. However, some values did fall

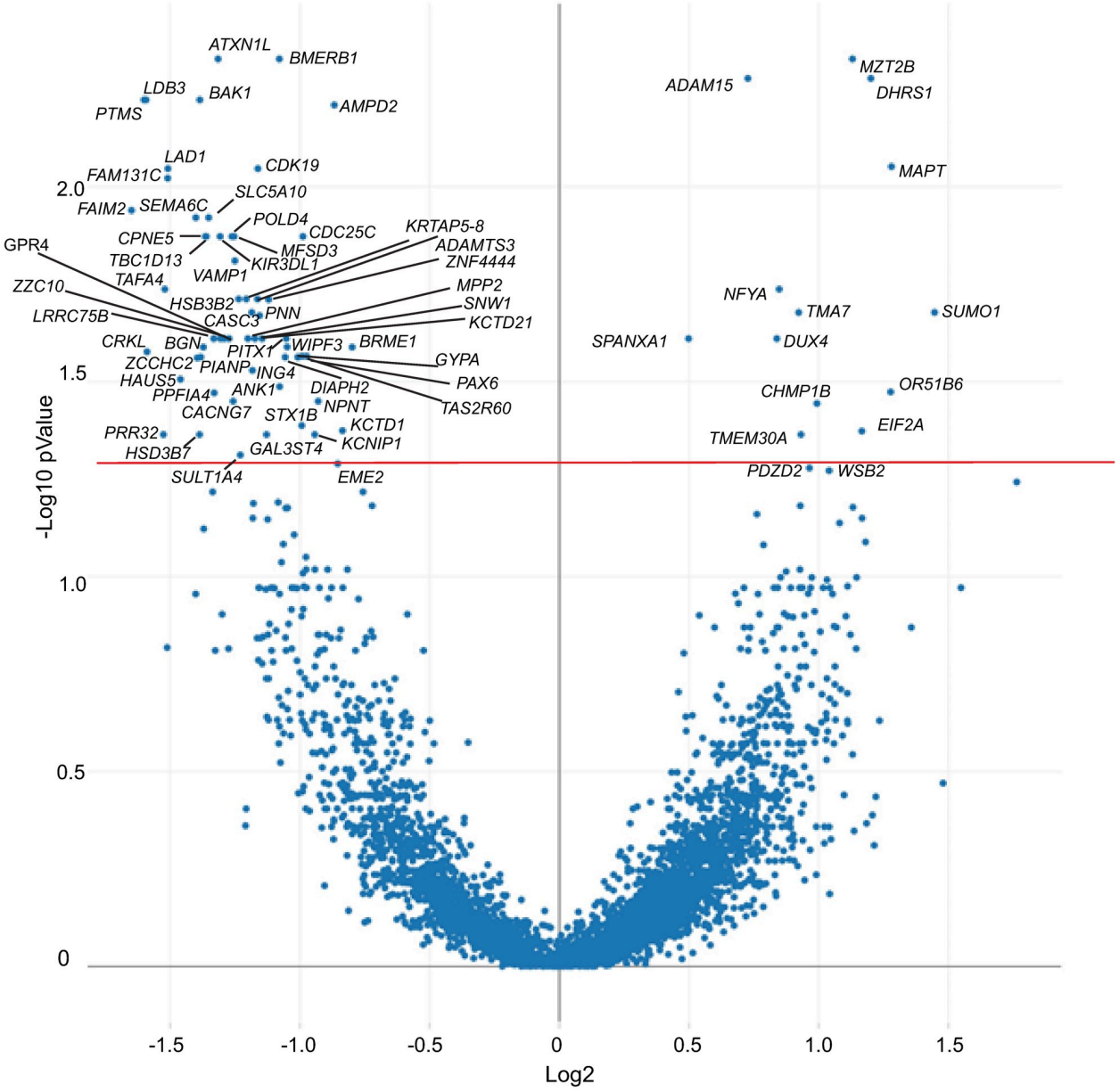

Fig 2. Volcano plot of differentially expressed genes. Plot shows differential expression of genes in high and low outflow areas. Each dot represents a specific gene. The solid horizontal red line shows the cutoff for genes with an adjusted p value <0.05. Only statistically significant genes are labeled.

https://doi.org/10.1371/journal.pone.0298802.g002

outside the IQR. These values, which were found within the lower or higher quartile ranges, indicated that there is some variability in the expression of these genes and that their expression is not uniformly distributed across the low or high outflow regions in the TM. The whisker boxplots of *ADAM15* and *LDB3* further demonstrated the variability in expression within segmental regions of outflow. For instance, the *ADAM15* data were skewed because most of the high outflow regions had high levels of *ADAM15* expression, but three regions fell in the lower quartile range outside the IQR. The whisker boxplot for *ADAM15* in the low outflow regions showed the opposite result. Most of the low flow regions showed low levels of ADAM15 expression, but two regions had higher levels of expression outside the IQR. The whisker boxplot for

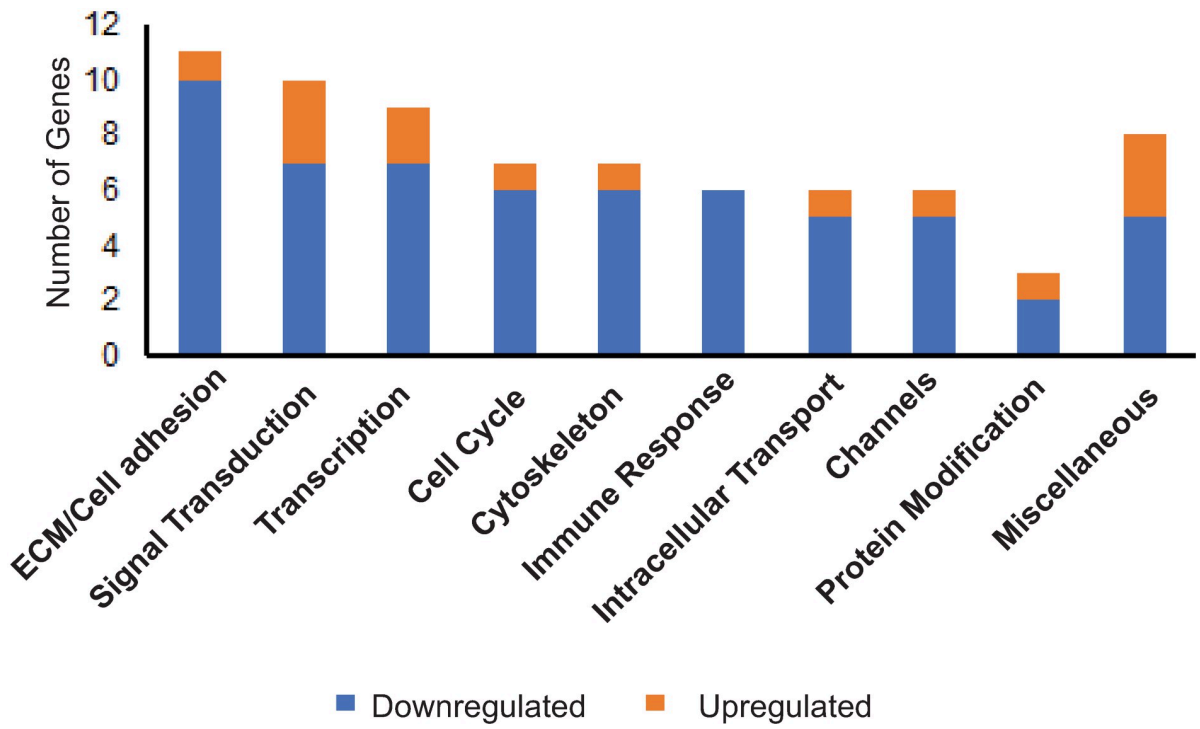

Fig 3. Biological categories of genes exhibiting differential expression in high outflow and low outflow regions of the TM. Biological processes were identified through gene ontology enrichment analysis using the following databases: DAVID Bioinformatics Resources, Gene Cards and UniProt.

https://doi.org/10.1371/journal.pone.0298802.g003

Table 1. ECM/cell adhesion genes differentially expressed compared to the high outflow regions. Unless otherwise noted with a citation, the function of genes was determined using GeneCards®, the human gene database or UniProtKB/Swiss site.

Gene	Protein Name	Function	Log2 FC	Adj p value
ADAM15	ADAM metallopeptidase domain 15	Metalloproteinase that binds β1 and β3 integrins and cleaves E-and N-cadherins and collagens	+0.7	0.005
SPANXA1	Sperm protein associated with the nucleus on the chromosome, family member A1	Suppresses EMT and upregulates E-cadherin expression [38]	+0.5	0.02
NPNT	Nephronectin	α8β1 integrin ligand	-1.0	0.04
GYPA	Glycophorin A	Pathogen receptor, impairs cell adhesion, may interact with integrins [39, 40]	-1.0	0.03
PNN	Pinin	Desmosome protein	-1.2	0.02
ADAMTS3	ADAM Metallopeptidase with Thrombospondin Type 1 Motif 3	Disintegrin and metalloproteinase; regulates type II collagen fibrillogenesis, cleaves VEGF-C [41]	-1.2	0.02
MPP2	MAGUK p55 scaffold protein 2	Organizes synapsis signaling with cell adhesion molecules	-1.2	0.03
GPR4	G protein-coupled receptor 4	Increases vascular permeability, VCAM mediated cell-cell adhesion; regulates focal adhesion dynamics. Pro-inflammatory receptor.	-1.3	0.02
PPFIA4	PTPRF interacting protein alpha 4 (Liprin-alpha)	Phosphatase; regulates disassembly of focal adhesions	-1.3	0.03
BGN	Biglycan	Small leucine-rich proteoglycan; crosslinks collagen fibrils and a DAMP for TLR4	-1.4	0.03
CRKL	CRK like proto-oncogene	Adaptor protein mediates focal adhesion formation, growth factor, integrin and cytokine signaling [42]	-1.6	0.03
LDB3	PDLIM6 (ZASP)	Stabilizes structural integrity of sarcomere during contraction; binds α-actinin; regulates α5β1 integrin activation [43]	-1.6	0.006

https://doi.org/10.1371/journal.pone.0298802.t001

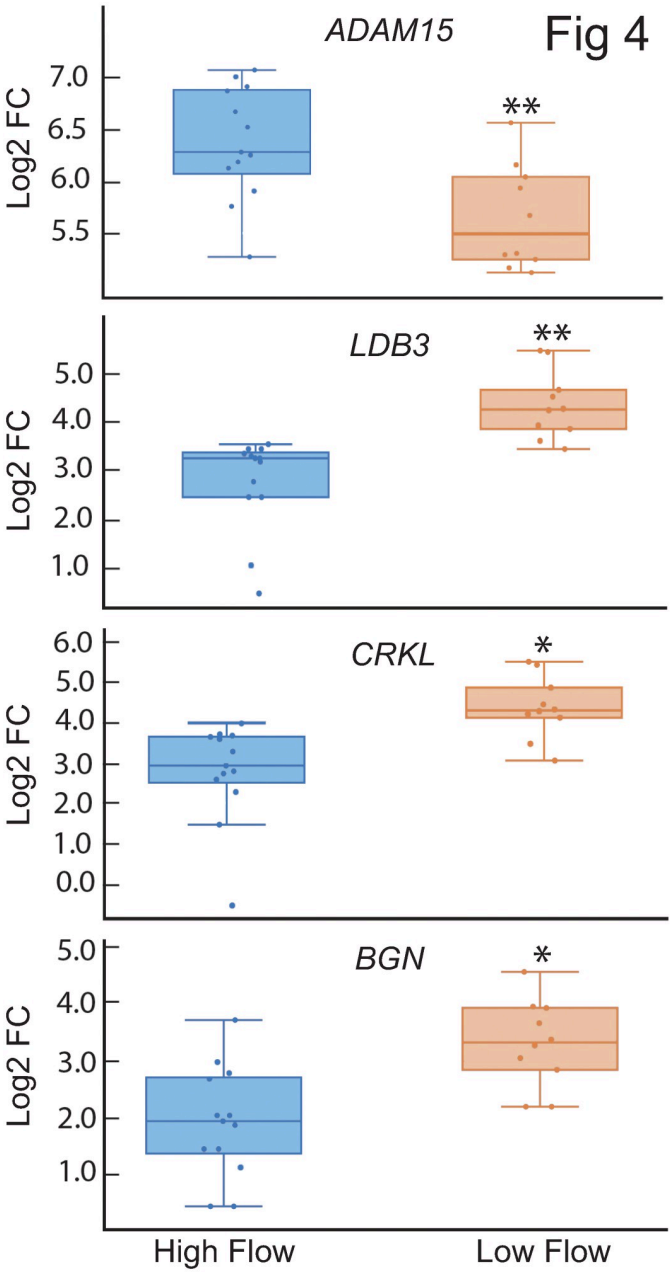

Fig 4. Box plots showing distribution of *ADAM15*, *LDB3*, *CRKL* and *BGN* gene expression in high and low outflow regions. Each dot represents the log2FC of the gene in one high or low outflow region. The horizontal bar represents the median of the log2FC for that gene within the interquartile range (IQR). The whiskers show the minimum and maximum log2FC change of that gene and its variability in comparison to the IQR as well as outliers. Points seen outside the box, but within the whiskers, represent data points that fall within the min (Q1-1.5* IQR) and max (Q3 + 1.5* IQR). Only data points outside the whiskers are considered outliers.

https://doi.org/10.1371/journal.pone.0298802.g004

LDB3 showed a similar distribution in low and high outflow regions. Together these data indicate the variability in gene expression within low or high outflow regions.

We did see that the data showed two outliers for *LDB3* and one outlier for *CRKL* in the high outflow segments. Further analysis showed that these outliers were from the same donor

(S1 Table). It is possible that this donor had fewer cells in those outflow regions which could account for the lower values. However, since neither *ADAM15* nor *BGN* contained outliers from these same donor tissue, this explanation is unlikely. Rather, the outliers seemed to be specific to *LDB3* and *CRKL* expression.

Immunofluorescence microscopy was then used to validate the protein expression of these genes in the TM. Out of these four proteins, only antibodies to ADAM15 were found to be available to label paraffin embedded tissues. As shown in Fig 5, this immunolabeling study showed that ADAM15 could be found in the TM. Labeling was detected in the trabecular beams, the JCT and the IW of Schlemm's Canal and appeared to be more highly expressed in these areas in high flow regions. To validate this, quantitative analysis of ADAM15 integrated density was done using Image J. This analysis showed that ADAM15 was more highly expressed in the JCT and IW of Schlemm's canal in high outflow areas compared to low outflow areas ($p<0.05$). It also appeared higher in the OW of Schlemm's canal in high outflow areas, but this difference was not statistically significantly different ($p>0.2$).

The next category of biological processes that appeared to have genes differentially expressed was signal transduction (Fig 3). Genes found in these categories are listed in Table 2. Interestingly, half of the genes involved in signal transduction events were involved in either Wnt signaling (*KCTD1*, *CDC25C*, *BGN*, *FAIM2* and *PTMS*), TGFβ signaling (*BGN*, *PTMS*) or glucocorticoid (*CXCL1*, *PTMS*) signaling all of which are signaling pathways known to be associated with controlling outflow facility and intraocular pressure [44–48].

The third category of biological processes that had differentially expressed genes was transcription (Fig 3). As shown in Table 3, only two transcription factors were upregulated in high outflow regions. Both *NFYA* and *DUX4* showed a fold change greater than 1.7 (log2FC = 0.8), and to the best of our knowledge, neither gene has been reported to be involved in segmental outflow. All the other transcription factors were downregulated. Among the transcription factors that were differentially downregulated in high outflow by 0.4-fold was *FOSL1* (log2FC = -1.3) and *ATXN1L* (log2FC = -1.3). *FOSL1* is a subunit of the AP-1 transcription factor and has been reported to be involved in epithelial-mesenchymal transition (EMT) and Wnt signaling [56, 57], both pathways associated with IOP [48]. *SNW1*, which is involved in TGFβ [58] and Wnt signaling [59], was also detected. *PAX6* (log2FC = -1.0) was also found to be downregulated in high flow regions. Interestingly, *PAX6* has previously been associated with glaucoma and *FOSL1*, which is associated with fibrosis, were both previously identified in an earlier study exploring the effect of αvβ3 integrin on the transcriptome of TM cells [60].

Finally, another category of note included genes associated with the cytoskeleton (S2 Table). As before, the majority of genes, with the exception of one gene (*MAPT*), were downregulated in high outflow regions compared to low outflow regions. *MAPT*, which encodes for the protein Tau, showed a log2FC = 1.3 or a 2.4-fold increase in expression in high outflow regions. Genes associated with the cytoskeleton that were differentially downregulated included *LDB*3 as discussed above and *LAD1* (log2FC = -1.6). *LAD1* encodes for the protein ladinin-1 which binds to filamin-bundled actin filaments. Ladinin-1 has only recently been found and studies suggest that it may play a role in the depolymerization of F-actin filaments via its association with filamin A [66]. Its association with filamin had also been shown to affect signaling and transcriptional networks and depletion of it causes slower rates of proliferation. All other genes identified in this study and the biological processes that they are associated with are listed in S2 Table.

Interestingly, none of the genes for ECM proteins (i.e *SPARC*, *VCAN*, *THBS2*, *FN1*, *DCN)* previously associated with affecting outflow facility [20, 21, 23, 25, 67, 68] were found to be statistically different between high and low outflow regions of the TM in this study (Fig 6). Nor did we see any statistical differences in the various integrins expressed in the low outflow

Fig 5

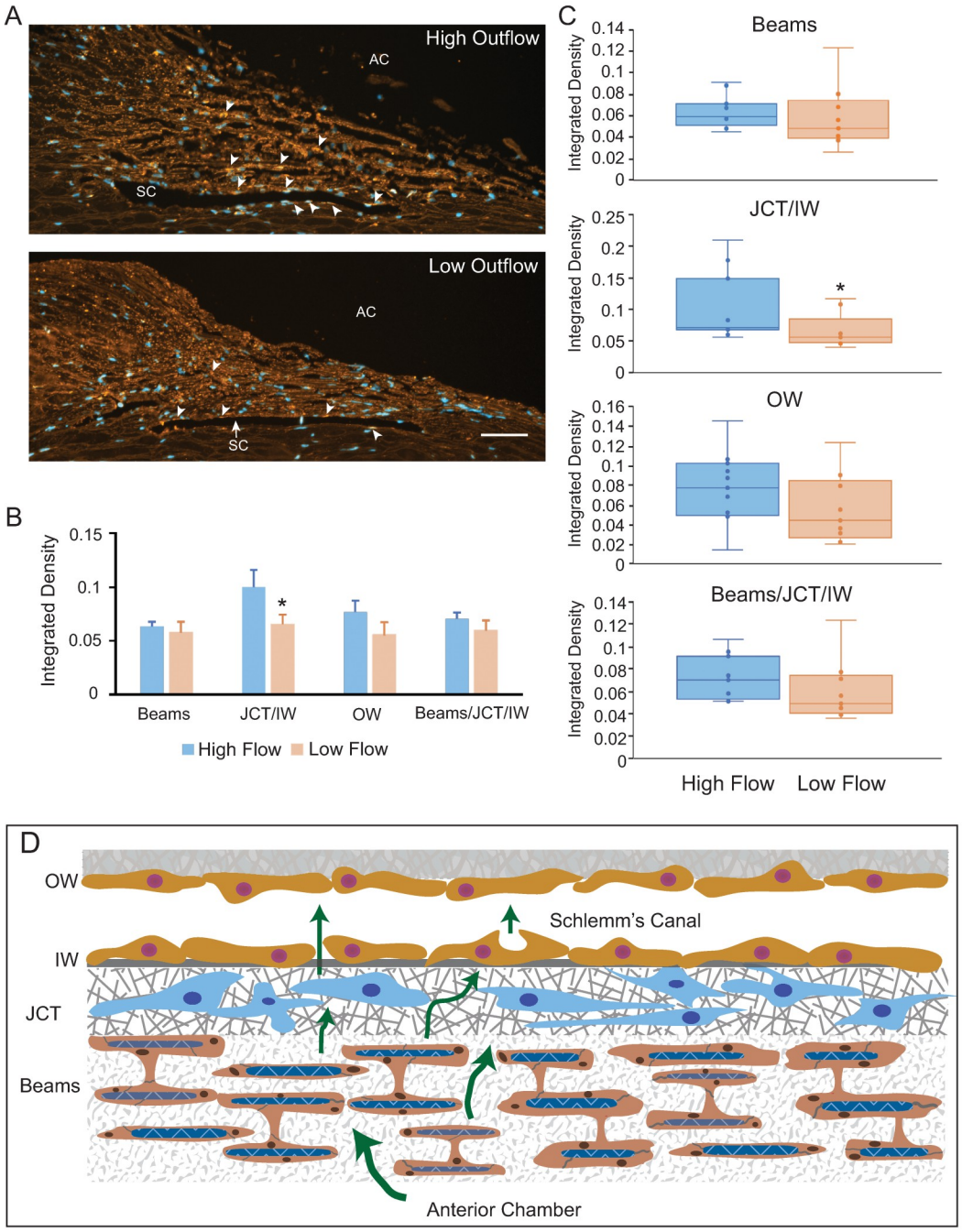

Fig 5. Localization of ADAM15 in high and low outflow segments of TM. (A) ADAM15 labeling (red) in high outflow regions and low outflow regions. AC, anterior chamber, SC, Schlemm's canal, Bar = 50μm. Arrowheads show ADAM15 in the beams and along Schlemm's canal. Sections were labeled with a rabbit monoclonal anti-ADAM15 antibody which was detected using Alexa 546-conjugated goat anti-rabbit IgG. Nuclei were labeled with Hoechst 33342 (blue). (B) Quantification of labeling along beams versus JCT/IW, OW and beams/JCT/IW in low and high outflow regions. * $p<0.05$ C) Box plots showing distribution of ADAM15 labeling in high and low outflow regions. Each dot represents the integrated density in one high or low outflow region. The horizontal bar represents the median of the integrated density. (D) Schematic of the trabecular meshwork/

Schlemm's canal outflow pathway. Aqueous humor (green arrows) flows through the trabecular beams and the JCT. It then crosses the IW of Schlemm's Canal to exit either paracellularly or transcellularly into the lumen of Schlemm's Canal and into the OW of Schlemm's Canal. The beams consist of a collagenous/elastic matrix surrounded by endothelial-like cells. The beams are connected to each other by cytoplasmic extensions between the cells surrounding the beams. IW, inner wall; OW outer wall, JCT, Juxtacanalicular region.

https://doi.org/10.1371/journal.pone.0298802.g005

versus high outflow regions of the TM (Fig 7) that are thought to regulate IOP [29, 69–71]. However, boxplot analysis of the distribution of the *DCN* and *ITGA8* integrin subunits did show an enrichment of these genes in high outflow regions compared to low outflow regions. The log2FC of these genes in each outflow segment is listed in S3 Table.

Table 2. Genes involved in signal transduction events. Unless otherwise noted with a citation, the function of genes was determined using GeneCards®, the human gene database or UniProtKB/Swiss site.

Gene	Protein Name	Function	Log2 FC	Adj p value
CXCL1	C-X-C Motif Chemokine Ligand 1	Glucocorticoid regulation; inflammation	+1.8	0.05
OR51B6	Olfactory Receptor Family 51 Subfamily B Member 6	G-protein receptor; transduction of odorant signals	+1.2	0.03
PDZD2	PDZ Domain Containing 2	ER protein; IL-16 similarity	+1.0	0.05
KCTD1	K2+ Channel Tetramerization Domain Containing 1	Modulation of Wnt signaling; enhances ubiquitination & degradation of β-catenin; represses transcriptional activity of AP-2	-0.8	0.04
CDC25C	Cell Division Cycle 25C	Mitosis, Wnt signaling pathway [49]	-1.0	0.01
TAS2R60	Taste 2 Receptor Member 60	G-protein coupled taste receptor; mediates PLC-beta-2 activation and gating of TRPM5	-1.0	0.0002
SEMA6C	Semaphorin 6C	Involved in neuromuscular communication [50], retinal development [51]; the AKT/GSK3/β-catenin/cyclin D1 pathway [52]	-1.4	0.01
BGN	Biglycan	Wnt and TGFβ signaling, collagen crosslinking	-1.4	0.03
TAFA4	TAFA chemokine like family member 4	Regulates immune or nervous cells in brain; promotes phagocytosis or ROS release in macrophages	-1.5	0.02
FAIM2	Fas Apoptotic Inhibitory Molecule 2	Regulates apoptosis and activates Wnt pathway [53]	-1.6	0.01
PTMS	Parathymosin (MTI-II)	Restores BMP4 signaling [54]; glucocorticoid co-receptor [55]	-1.6	0.006

https://doi.org/10.1371/journal.pone.0298802.t002

Table 3. Genes involved in transcription. Unless otherwise noted with a citation, the function of genes was determined using GeneCards®, the human gene database or UniProtKB/Swiss site.

Gene	Protein Name	Function	Log2 FC	Adj p value
NFYA	Nuclear transcription factor Y subunit alpha	CCAAT binding transcription factor; regulates lipid metabolism and gluconeogenesis [61]	+0.8	0.01
DUX4	Double homeobox 4	Transcriptional activator of PITX1, may regulate miRNA expression	+0.8	0.02
PAX6	Paired box 6	Eye development; regulates VEGF, α4, and α5 integrin expression [62]	-1.0	0.03
PITX1	Paired like homeodomain 1	Transcription factor; regulates apoptosis-related genes (ZCCHH10 and htert) and hind limb development, [63, 64]	-1.1	0.02
ZNF444	Zinc finger protein 444	Activates transcription of a scavenger receptor gene involved in the degradation of Ac-LDL	-1.1	0.02
CASC3	CASC3 exon junction complex subunit;	Component of spliceosome	-1.2	0.02
SNW1	SNW domain containing 1	Splicing and transcription, modulates TGFβ mediated transcription via Smads, coactivator that enhances glucocorticoid-mediated gene expression.	-1.2	0.02
ATXN1L	Ataxin 1 like	Regulates transcription; represses notch signaling	-1.3	0.005
FOSL1	FOS like 1	AP-1 transcription factor subunit; promotes EMT and Wnt signaling [65]	-1.3	0.02

https://doi.org/10.1371/journal.pone.0298802.t003

Fig 6

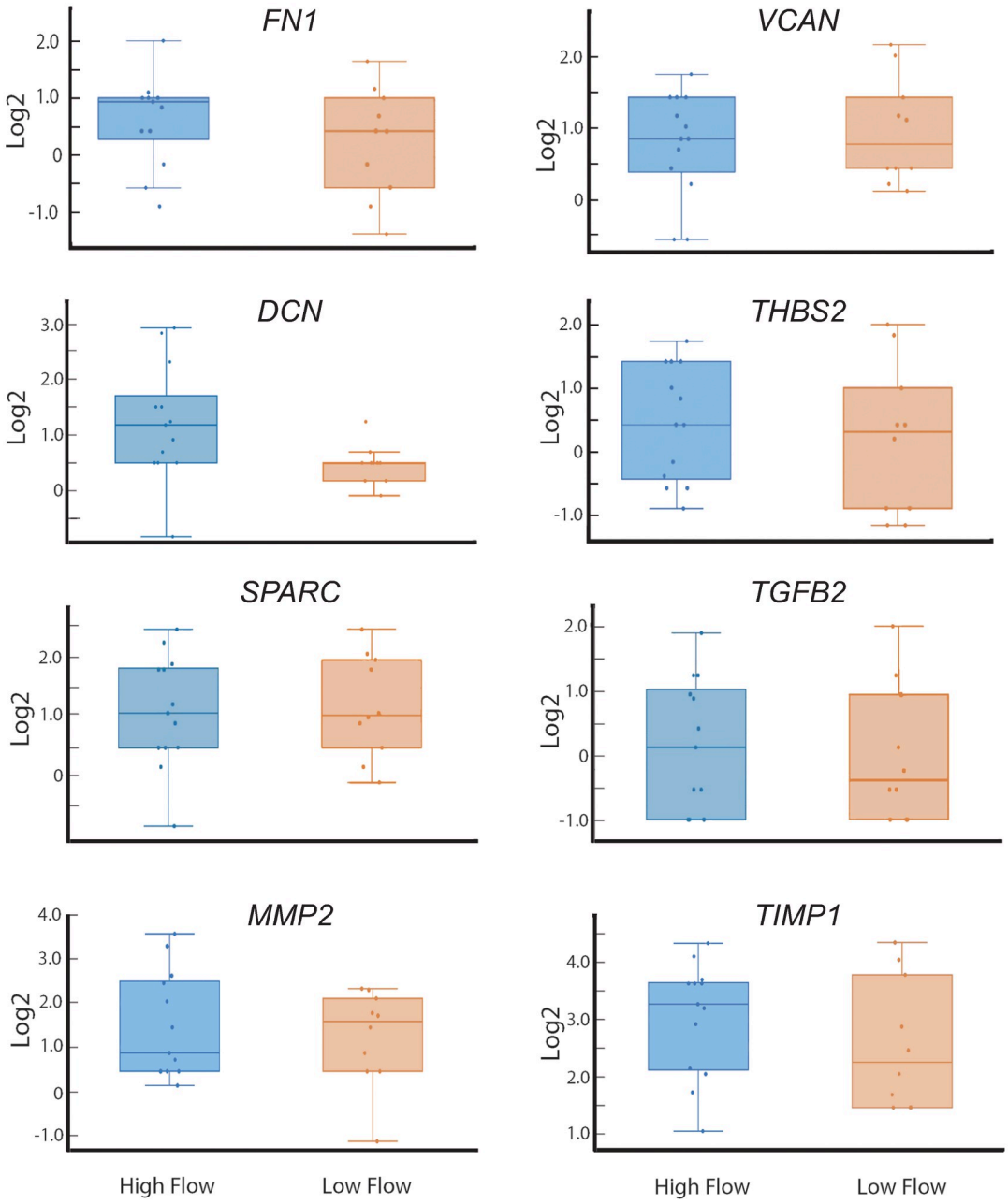

Fig 6. Box plots showing distribution of various ECM genes and *TGF*β2 in high and low outflow regions. Each dot represents the log2FC of the gene in one high or low outflow region. *DCN* was the only gene which showed a preferential distribution to the high outflow region of the TM. The horizontal bar represents the median of the log2FC for that gene within the IQR. The whiskers show the minimum and maximum log2FC change of that gene and its variability in comparison to the IQR as well as outliers. Points seen outside the box but within the whiskers represent data points that fall within the min (Q1-1.5* IQR) and max (Q3 + 1.5* IQR). Only data points outside the whiskers are considered outliers. *FN1*, fibronectin; *VCAN*, versican, *DCN*, decorin; *THBS2*, thrombospondin 2; *MMP2*, matrix metalloproteinase 2; *TGFB2*, transforming growth factor 2; *TIMP1*, TIMP metallopeptidase inhibitor 1.

https://doi.org/10.1371/journal.pone.0298802.g006

Fig 7

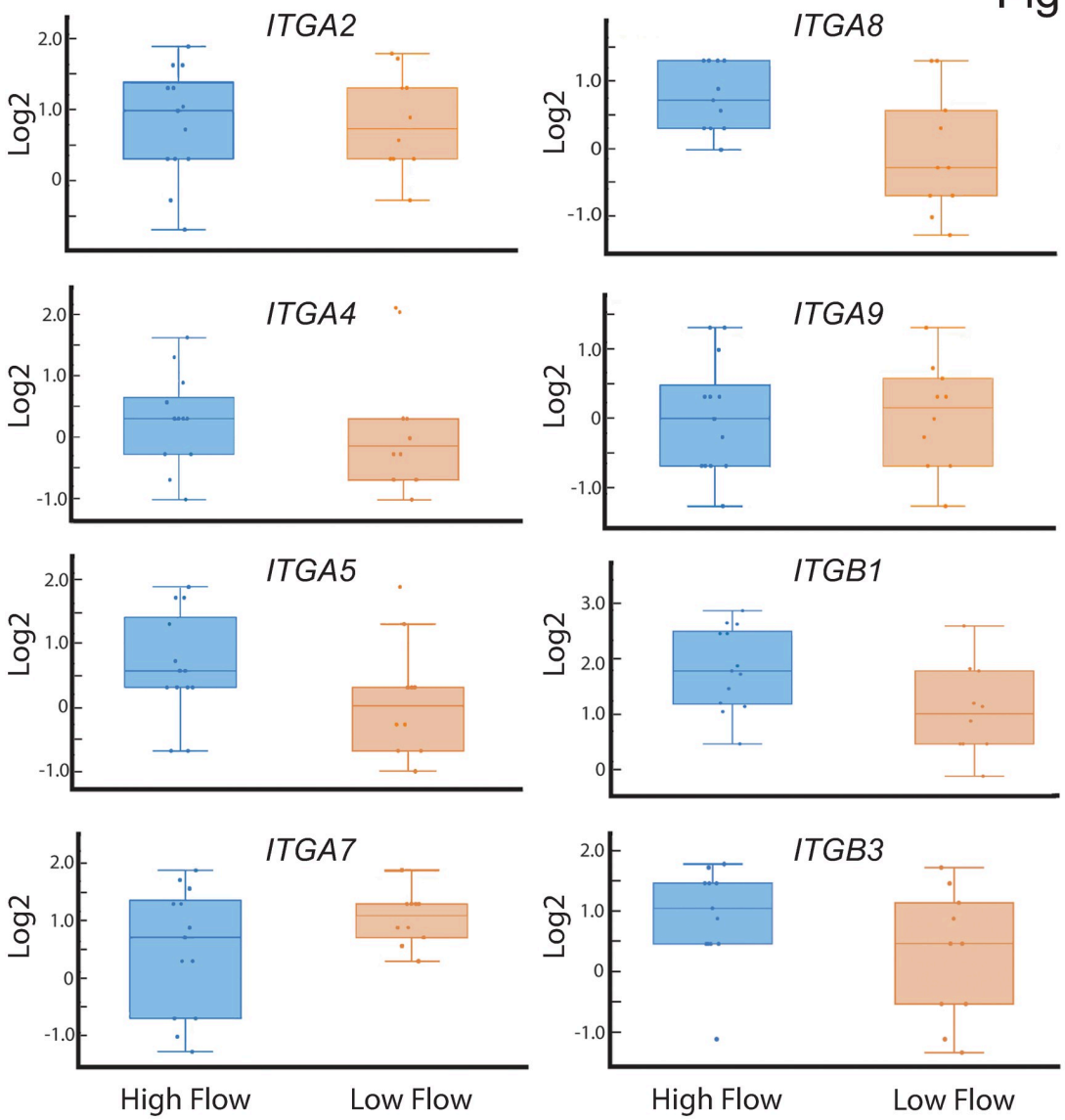

Fig 7. Box plots showing distribution of various integrin genes in high and low outflow regions. Each dot represents the log2FC of the gene in one high or low outflow region. Of all these integrins, only the *ITGA8* showed enrichment in the high outflow regions of the TM. The horizontal bar represents the median of the log2FC for that gene within the IQR. The whiskers show the minimum and maximum log2 FC change of that gene and its variability in comparison to the IQR as well as outliers. Points seen outside the box but within the whiskers represent data points that fall within the min (Q1-1.5* IQR) and max (Q3 + 1.5* IQR). Only data points outside the whiskers are considered outliers. *ITGA2*, α2 integrin; *ITGA4*, α4 integrin; *ITGA5*, α5 integrin; *ITGA7*, α7 integrin; *ITGA8*, α8 integrin; *ITGA9*, α9 integrin; *ITGB1*, β1 integrin; *ITGB3*, β3 integrin.

https://doi.org/10.1371/journal.pone.0298802.g007

Discussion

Using digital spatial profiling of the transcriptome of high and low outflow regions of human anterior segments, this study identified several previously unidentified genes that could be associated with segmental outflow. Many of the genes identified were not the major structural ECM proteins in the TM ECM. Rather the genes identified in this study regulated cell adhesion and/or the organization of the ECM supporting the idea that ECM organization is the critical mediator for segmental outflow [13, 31, 67].

Interestingly, the fold changes in expression of these genes were relatively small suggesting that segmental outflow is unlikely to be regulated by substantial changes in the expression of ECM genes. Previous proteomic studies [30] support this idea as the differential expression of ECM proteins in low and high outflow regions could only be detected when anterior segments were exposed to elevated pressure even though segmental outflow was detected at physiological pressure. This suggests that major changes in gene and protein expression are unlikely to account for segmental flow at physiological pressures and it is the activity or structural arrangement of ECM proteins that probably account for segmental outflow.

One of the genes identified in this study was *ADAM15*. *ADAM15* is a member of the disintegrin-metalloproteinase family and is best known for its role in cartilage homeostasis and tissue remodeling in vascular and cardiac tissues [72–74]. It has recently been suggested to orchestrate a novel pro-inflammatory mechanosensing pathway in synovial fibroblasts [75] and to play a role in regulating TGFβ signaling in cartilage [76]. Furthermore, it may modulate the activity of SLC26A2, which is a sulfate transporter responsible for maintaining adequate sulfation of proteoglycans [77]. This latter activity is intriguing since glycosaminoglycan sulfation plays an important role in the TM ECM [78–80], and it can affect the assembly of the fibronectin matrix [81], BMP-2 and TGFβ1 bioavailability and modulate signals from cell–cell and cell–ECM interactions [82]. ADAM15 also binds α9β1 and αvβ3 integrins [83, 84] and regulates αvβ3 and α7β1 integrin signaling [85, 86]. It also acts as a mechanosensory protein associated with TRPV4 Ca2+ channels [75, 87] and is upregulated by shear stress [87]. Thus, in conjugation with integrins, an ADAM15/integrin signaling complex should be able to sense elevated IOP and changes to the biomechanical environment, thereby transmitting mechanical signals intracellularly.

Together, the signaling and proteolytic activities of ADAM15, and its known association with a number of proteins/process relevant to controlling the movement of aqueous humor through the TM/SC, strongly suggest that ADAM15 can play a vital role in regulating outflow facility and the permeability of Schlemm's canal. Whether it is involved in glaucoma is still unclear. However, ADAM15 was shown to be a binding partner and target for the podosomal-adaptor protein SH3PXD2B that is mutated in the *nee* mouse model of glaucoma [88, 89]. Podosome-like structures control focal ECM turnover in TM cells [90]. Thus, any changes in ADAM15 expression could affect the podosomal degradative activity thereby affecting aqueous humor outflow through the TM [90]. Further studies examining ADAM15 levels in glaucomatous cells and tissues are clearly warranted.

Notably, previous studies have shown that another member of this family, ADAMTS4, affected outflow in human anterior segment perfusion culture [91], and perfusion of recombinant ADAMTS4 into either human or porcine anterior segments significantly increased pressure. Levels of ADAMTS4 expression were also elevated in the JCT region of the TM when anterior segments were perfused at increased pressure. Hence *ADAM15* and this family of proteins has the potential to create a microenvironment critical for TM homeostasis.

One of the striking findings of this study was the observation that none of the ECM proteins [20, 21, 23, 25, 67, 68] and integrins [29, 69–71] previously identified to affect IOP or outflow showed any significant differences in gene expression between low and high outflow regions. As shown in the boxplots for these genes and S3 Table, there was a lot of variation in the expression of genes within a high or low flow region that could not be attributed to the donor eye. For instance, in the box plot showing fibronectin expression in the high outflow regions, one particular high outflow region had the highest level of expression, while another high outflow region from the same eye had the lowest level of fibronectin expression. It should be noted, however, that this does not negate the importance of these genes in outflow facility. It simply means that differences in gene expression does not necessarily explain their

importance. Clearly, the activity of the protein [95–97] and any post-translation modifications [17, 37] as well as interactions with neighboring proteins in signaling complexes [96, 98] could be driving their role in outflow facility.

Another explanation for why a differential expression of these ECM genes was not detected could be due to the approach used to identify genes, i.e. a digital profiling technique versus isolation of RNA from dissected tissue. In addition, many of those ECM proteins were previously identified by overexpressing or knocking out a protein. In this scenario, however, the effect on segmental outflow and/or IOP is just as likely to be due to altering the 3-D structural function of the ECM as is the change in expression of one protein. Studies using artificial collagen scaffolds support this idea and show that the pore architecture of a collagen gel and glycosaminoglycan composition affects human TM cell behavior [80, 92] while the physical attributes of type I collagen fibrils in gels affects cell adhesion, integrin activation and contractility [93, 94]. This suggests that the local microarchitecture of the ECM in high and low outflow areas, and not differences in ECM protein expression, could be just as critical for regulating segmental outflow as protein levels.

Although we didn't see a differential expression of *DCN* and *ITGA8* that was statistically significant under the statistical parameters used, it is interesting that we did see an enrichment of the *DCN* gene expression in high outflow regions. Previous studies have shown that decorin expression is associated with lower IOP in a rat model of glaucoma (68) and decorin-deficient mice exhibited a higher IOP [26]. Decorin, a known antagonist of TGFβ signaling, could potentially affect outflow by attenuating the expression of TGFβ2 and target genes of the TGFβ signaling pathway [26]. The enrichment of *ITGA8* in high outflow regions is also an interesting finding. *ITGA8* is associated with vascular smooth muscle cells [95, 96] or cells that have contractile functions. This suggests that it could be involved in mediating the contractile properties of TM and/or SC cells. In vitro studies in mesenchymal cells have shown that a lack of *ITGA8* causes a loss of actin stress fibers and reorganization of the cytoskeleton [97] which could result in reduced contractility of the cell. These findings are supported by data obtained from vascular smooth muscle cells, where *ITGA8* expression promotes the contractile phenotype [98].

Interestingly, *NPNT*, which is reported to be a ligand for *ITGA8* [99] was found to be significantly decreased in high outflow regions (Table 1). This suggests that interactions between *NPNT* and *ITGA8* could be responsible for regulating outflow. For instance, changes in *NPNT* expression could induce *ITGA8* activity that may reduce outflow by controlling the contractility of TM cells.

In summary, this study shows that digital spatial profiling is a useful approach to study genes that affect outflow facility, and it has identified a number of novel, differentially expressed genes whose expression could affect segmental outflow. Many of these genes are involved in regulating cell adhesion, ECM formation and/or Wnt/TGFβ signaling suggesting that segmental outflow is likely to be regulated by the activity of the ECM and cell adhesion molecules in the TM. Clearly, additional studies examining the expression and activity of the proteins expressed by these genes are warranted.

Supporting information

S1 Table. Log2FC values for each segment in high and low outflow regions of TM.
(DOCX)

S2 Table. Genes differentially expressed in high outflow regions of TM.
(DOCX)

S3 Table. Log2FC values of ECM proteins and integrins for each segment in high and low outflow regions of TM.
(DOCX)

S1 File.
(PDF)

Acknowledgments

The authors thank the University of Wisconsin Translational Research Initiatives in Pathology laboratory (TRIP) for their assistance with these studies.

Author Contributions

Conceptualization: Kate E. Keller, Donna M. Peters.

Data curation: Jennifer A. Faralli, Kate E. Keller, Donna M. Peters.

Formal analysis: Jennifer A. Faralli, Yong-Feng Yang, Donna M. Peters.

Funding acquisition: Kate E. Keller, Donna M. Peters.

Investigation: Jennifer A. Faralli, Mark S. Filla, Yong-Feng Yang, Ying Ying Sun.

Methodology: Kate E. Keller, Donna M. Peters.

Project administration: Donna M. Peters.

Resources: Kate E. Keller, Donna M. Peters.

Supervision: Kate E. Keller, Donna M. Peters.

Validation: Jennifer A. Faralli, Mark S. Filla.

Visualization: Donna M. Peters.

Writing – original draft: Donna M. Peters.

Writing – review & editing: Jennifer A. Faralli, Mark S. Filla, Kassidy Johns, Kate E. Keller.

References

1. Grant WM. Facility of flow through the trabecular meshwork. 1955; 54:245–8. https://doi.org/10.1001/archopht.1955.00930020251012 PMID: 14397911
2. Grant WM. Experimental aqueous perfusion in enucleated human eyes. Arch Ophthalmol. 1963; 69:783–801. https://doi.org/10.1001/archopht.1963.00960040789022 PMID: 13949877
3. Acott TS, Vranka JA, Keller KE, Raghunathan VK, Kelley MJ. Normal and glaucomatous outflow regulation. Prog Retin Eye Res. 2021; 82:100897. https://doi.org/10.1016/j.preteyeres.2020.100897 PMID: 32795516
4. Johnson M. What controls aqueous humour outflow resistance?. Exp Eye Res. 2006; 82:545–57. https://doi.org/10.1016/j.exer.2005.10.011 PMID: 16386733
5. Buller C, Johnson D. Segmental variability of the trabecular meshwork in normal and glaucomatous eyes. Invest Ophthalmol Vis Sci. 1994; 35:3841–51. PMID: 7928181
6. Hann CR, Bahler CK, Johnson DH. Cationic ferritin and segmental flow through the trabecular meshwork. Invest Ophthalmol Vis Sci. 2005; 46:1–7. https://doi.org/10.1167/iovs.04-0800 PMID: 15623746
7. Swaminathan SS, Oh D-J, Kang MH, Rhee DJ. Aqueous outflow: segmental and distal flow. J Cataract Refract Surg. 2014; 40:1263–72. https://doi.org/10.1016/j.jcrs.2014.06.020 PMID: 25088623
8. Saraswathy S, Tan JCH, Yu F, Francis BA, Hinton DR, Weinreb RN, et al. Aqueous angiography: real-time and physiologic aqueous humor outflow imaging. PLoS One. 2016; 11:e0147176. https://doi.org/10.1371/journal.pone.0147176 PMID: 26807586

9. Hann CR, Fautsch MP. Preferential fluid flow in the human trabecular meshwork near collector channels. Invest Ophthalmol Vis Sci. 2009; 50:1692–7. https://doi.org/10.1167/iovs.08-2375 PMID: 19060275

10. Chang JYH, Folz SJ, Laryea SN, Overby DR. Multi-scale analysis of segmental outflow patterns in human trabecular meshwork with changing intraocular pressure. JOPT. 2014; 30:213–23. https://doi.org/10.1089/jop.2013.0182 PMID: 24456518

11. Cha EDK, Xi J, Gong L, Gong H. Variations in active outflow along the trabecular outflow pathway. Exp Eye Res. 2016; 146:354–60. https://doi.org/10.1016/j.exer.2016.01.008 PMID: 26775054

12. Swain DL, Le TD, Yasmin S, Fernandes B, Lamaj G, Dasgupta I, et al. Morphological factors associated with giant vacuoles with I-pores in Schlemm's canal endothelial cells of human eyes: A serial block-face scanning electron microscopy study. Exp Eye Res. 2021; 205:108488. https://doi.org/10.1016/j.exer.2021.108488 PMID: 33571532

13. Vranka JA, Staverosky JA, Raghunathan VK, Acott TS. Elevated pressure influences relative distribution of segmental regions of the trabecular meshwork. Exp Eye Res. 2020; 190:107888. https://doi.org/10.1016/j.exer.2019.107888 PMID: 31786158

14. Reina-Torres E, Baptiste TMG, Overby DR. Segmental outflow dynamics in the trabecular meshwork of living mice. Exp Eye Res. 2022; 225:109285. https://doi.org/10.1016/j.exer.2022.109285 PMID: 36273576

15. Bradley JM, Vranka J, Colvis CM, Conger DM, Alexander JP, Fisk AS, et al. Effect of matrix metalloproteinases activity on outflow in perfused human organ culture. Invest Ophthamol Vis Sci. 1998; 39 (13):2649–58. PMID: 9856774

16. Ethier CR. The inner wall of Schlemm's canal. Exp Eye Res. 2002; 74:161–72. https://doi.org/10.1006/exer.2002.1144 PMID: 11950226

17. Keller KE, Peters DM. Pathogenesis of glaucoma: Extracellular matrix dysfunction in the trabecular meshwork—A review. Clin Experiment Ophthalmol. 2022; 50:163–82. https://doi.org/10.1111/ceo.14027 PMID: 35037377

18. Acott TS, Kelley MJ. Extracellular matrix in the trabecular meshwork. Exp Eye Res. 2008; 86:543–61. https://doi.org/10.1016/j.exer.2008.01.013 PMID: 18313051

19. Tamm ER. The trabecular meshwork outflow pathways: structural and functional aspects. Exp Eye Res. 2009; 88:648–55. https://doi.org/10.1016/j.exer.2009.02.007 PMID: 19239914

20. Faralli JA, Filla MS, McDowell CM, Peters DM. Disruption of fibronectin fibrillogenesis affects intraocular pressure (IOP) in BALB/cJ mice. PLoS One. 2020; 15:e0237932. https://doi.org/10.1371/journal.pone.0237932 PMID: 32822410

21. Roberts AL, Mavlyutov TA, Perlmutter TE, Curry SM, Harris SL, Chauhan AK, et al. Fibronectin extra domain A (FN-EDA) elevates intraocular pressure through Toll-like receptor 4 signaling. Sci Rep. 2020; 10:9815. https://doi.org/10.1038/s41598-020-66756-6 PMID: 32555351

22. Aihara M, Lindsey JD, Weinreb RN. Ocular hypertension in mice with a targeted type I collagen mutation. Invest Ophthamol Vis Sci. 2003; 44:1581–5. https://doi.org/10.1167/iovs.02-0759 PMID: 12657595

23. Haddadin RI, Oh DJ, Kang MH, Filippopoulos T, Gupta M, Hart L, et al. SPARC-null mice exhibit lower intraocular pressures. Invest Ophthalmol Vis Sci. 2009; 50:3771–7. https://doi.org/10.1167/iovs.08-2489 PMID: 19168904

24. Oh D-J, Kang MH, Ooi YH, Choi KR, Sage EH, Rhee DJ. Overexpression of SPARC in human trabecular meshwork increases intraocular pressure and alters extracellular matrix. Invest Ophthalmol Vis Sci. 2013; 54:3309–19. https://doi.org/10.1167/iovs.12-11362 PMID: 23599341

25. Haddadin R, Oh D, Kang M, Villarreal GJ, Kang J, Jin R, et al. Thrombospondin-1 (TSP1)-null and TSP2-null mice exhibit lower intraocular pressures. Invest Ophthamol Vis Sci. 2012; 53:6708–17. https://doi.org/10.1167/iovs.11-9013 PMID: 22930728

26. Schneider M, Pawlak R, Weber GR, Dillinger AE, Kuespert S, Iozzo RV, et al. A novel ocular function for decorin in the aqueous humor outflow. Matrix Biol. 2021; 97:1–19. https://doi.org/10.1016/j.matbio.2021.02.002 PMID: 33582236

27. Senatorov V, Malyukova I, Fariss R, Wawrousek EF, Swaminathan S, Sharan SK, et al. Expression of mutated mouse myocilin induces open-angle glaucoma in transgenic mice. J Neurosci. 2006; 26:11903–14. https://doi.org/10.1523/JNEUROSCI.3020-06.2006 PMID: 17108164

28. Cheng Y, Wu S, Yan X, Liu Q, Lin D, Zhang J, et al. Human Pro370Leu mutant myocilin induces the phenotype of open-angle glaucoma in transgenic mice. Cell Mol Neurobiol. 2022; 43:2021–33. https://doi.org/10.1007/s10571-022-01280-x PMID: 36069958

29. Vranka JA, Acott TS. Pressure-induced expression changes in segmental flow regions of the human trabecular meshwork. Exp Eye Res. 2017; 158:67–72. https://doi.org/10.1016/j.exer.2016.06.009 PMID: 27334250

30. Vranka JA, Staverosky JA, Reddy AP, Wilmarth PA, David LL, Acott TS, et al. Biomechanical rigidity and quantitative proteomics analysis of segmental regions of the trabecular meshwork at physiologic and elevated pressures. Invest Ophthalmol Vis Sci. 2018; 59:246–59. https://doi.org/10.1167/iovs.17-22759 PMID: 29340639

31. Vranka JA, Bradley JM, Yang YF, Keller KE, Acott TS. Mapping molecular differences and extracellular matrix gene expression in segmental outflow pathways of the human ocular trabecular meshwork. PloS One. 2015; 10(3):e0122483. https://doi.org/10.1371/journal.pone.0122483 PMID: 25826404

32. Saraswathy S, Bogarin T, Barron E, Francis BA, Tan JCH, Weinreb RN, et al. Segmental differences found in aqueous angiographic-determined high—and low-flow regions of human trabecular meshwork. Exp Eye Res. 2020; 196:108064. https://doi.org/10.1016/j.exer.2020.108064 PMID: 32439396

33. Staverosky J, Dhamodaran K, Acott T, Raghunathan V, Vranka J. Isolation and characterization of primary human trabecular meshwork cells from segmental flow regions: New tools for understanding segmental flow. Exp Eye Res. 2020; 197:108046. https://doi.org/10.1016/j.exer.2020.108046 PMID: 32376472

34. Kuehn MH, Vranka JA, Wadkins D, Jackson T, Cheng L, Ledolter J. Circumferential trabecular meshwork cell density in the human eye. Exp Eye Res. 2021; 205:108494. https://doi.org/10.1016/j.exer.2021.108494 PMID: 33596442

35. Strohmaier CA, McDonnell FS, Zhang X, Wanderer D, Stamer WD, Weinreb RN, et al. Differences in outflow facility between angiographically identified high- versus low-flow regions of the conventional outflow pathways in porcine eyes. Invest Ophthalmol Vis Sci. 2023; 64:29. https://doi.org/10.1167/iovs.64.3.29 PMID: 36939719

36. Acott TS, Kingsley PD, Samples JR, Van Buskirk EM. Human trabecular meshwork organ culture: morphology and glycosaminoglycan synthesis. Invest Ophthalmol Vis Sci. 1988; 29:90–100. PMID: 3335436

37. Keller KE, Bradley JM, Kelley MJ, Acott TS. Effects of Modifiers of Glycosaminoglycan Biosynthesis on Outflow Facility in Perfusion Culture. Invest Ophthamol Vis Sci. 2008; 49:2495–505. https://doi.org/10.1167/iovs.07-0903 PMID: 18515587

38. Hsiao Y-J, Su K-Y, Hsu Y-C, Change G-C, Chen J-S, Chen H-Y, et al. SPANXA suppresses EMT by inhibiting c-JUN/SNAI2 signaling in lung adenocarcinoma. Oncotarget. 2016; 7:44417–29. https://doi.org/10.18632/oncotarget.10088 PMID: 27323831

39. Poole J. Red cell antigens on band 3 and glycophorin A. Blood Rev. 2000; 14:31–43. https://doi.org/10.1054/blre.1999.0124 PMID: 10805259

40. Schneider D, Engelman DM. Involvement of transmembrane domain interactions in signal transduction by α/β integrins. J Biol Chem. 2004; 279:9840–6. https://doi.org/10.1074/jbc.M312749200 PMID: 14681217

41. Bui HM, Enis D, Robciuc MR, Nurmi HJ, Cohen J, Chen M, et al. Proteolytic activation defines distinct lymphangiogenic mechanisms for VEGFC and VEGFD. JCI. 2016; 126:2167–80. https://doi.org/10.1172/JCI83967 PMID: 27159393

42. Li L, Guris DL, Okura M, Imamoto A. Translocation of CrkL to focal Adhesions mediates integrin-induced migration downstream of Src family kinases. Mol Cell Biol. 2003; 23:2883–92. https://doi.org/10.1128/MCB.23.8.2883-2892.2003 PMID: 12665586

43. Bouaouina M, Jani K, Long JY, Czerniecki S, Morse EM, Ellis SJ, et al. Zasp regulates integrin activation J Cell Sci. 2012; 125:5647–57. https://doi.org/10.1242/jcs.103291 PMID: 22992465

44. Clark A, Wordinger RJ. The role of steroids in outflow resistance. Exp Eye Res. 2009; 88:752–9. https://doi.org/10.1016/j.exer.2008.10.004 PMID: 18977348

45. Wordinger RJ, Sharma T, Clark AF. The role of TGF-β2 and bone morphogenetic proteins in the trabecular meshwork and glaucoma. JOPT. 2014; 30:154–62. https://doi.org/10.1089/jop.2013.0220 PMID: 24517218

46. Braunger BM, Fuchshofer R, Tamm ER. The aqueous humor outflow pathways in glaucoma: A unifying concept of disease mechanisms and causative treatment. Eur J Pharm Biopharm. 2015; 95, Part B:173–81. https://doi.org/10.1016/j.ejpb.2015.04.029 PMID: 25957840

47. Webber HC, Bermudez JY, Sethi A, Clark AF, Mao W. Crosstalk between TGFβ and Wnt signaling pathways in the human trabecular meshwork. Exp Eye Res. 2016; 148:97–102. https://doi.org/10.1016/j.exer.2016.04.007 PMID: 27091054

48. Sugali CK, Payana NP, Dai J, Peng M, Harris SL, Webber HC, et al. The canonical Wnt signaling pathway inhibits the glucocorticoid receptor signaling pathway in the trabecular meshwork. Am J Pathol. 2021; 191:1020–35. https://doi.org/10.1016/j.ajpath.2021.02.018 PMID: 33705750

49. Davidson G, Shen J, Huang YL, Su Y, Karaulanov E, Bartscherer K, et al. Cell cycle control of wnt receptor activation. Dev Cell. 2009; 17:788–99. https://doi.org/10.1016/j.devcel.2009.11.006 PMID: 20059949

50. Svensson A, Libelius R, Tagerud S. Semaphorin 6C expression in innervated and denervated skeletal muscle. J Mol Histol. 2008; 39:5–13. https://doi.org/10.1007/s10735-007-9113-6 PMID: 17605078

51. Matsuoka RL, Sun LO, Katayama K, Yoshida Y, Kolodkin AL. Sema6B, Sema6C, and Sema6D expression and function during mammalian retinal development. PloS One. 2013; 8:e63207. https://doi.org/10.1371/journal.pone.0063207 PMID: 23646199

52. Hung Y-H, Hsu S-H, Hou Y-C, Chu P-Y, Su Y-Y, Shan Y-S, et al. Semaphorin 6C suppresses proliferation of pancreatic cancer cells via inhibition of the AKT/GSK3/β-catenin/cyclin D1 pathway. Int J Mol Sci. 2022; 23:2608. https://doi.org/10.3390/ijms23052608 PMID: 35269749

53. She K, Yang W, Li M, Xiong W, Zhou M. FAIM2 promotes mon-small cell lung cancer cell growth and bone metastasis by activating the Wnt/β-catenin pathway. Front Oncol. 2021; 11:690142. https://doi.org/10.3389/fonc.2021.690142 PMID: 34568020

54. Hirata-Tsuchiya S, Suzuki S, Okamoto K, Saito N, Yuan H, Yamada S, et al. A small nuclear acidic protein (MTI-II, Zn2+-binding protein, parathymosin) attenuates TNF-α inhibition of BMP-induced osteogenesis by enhancing accessibility of the Smad4-NF-κB p65 complex to Smad binding element. Mol Cell Biochem. 2020; 469:133–42. https://doi.org/10.1007/s11010-020-03734-6 PMID: 32304006

55. Okamoto K, Isohashi F. Macromolecular translocation inhibitor II (Zn(2+)-binding protein, parathymosin) interacts with the glucocorticoid receptor and enhances transcription in vivo. J Biol Chem. 2005; 280:36986–93. https://doi.org/10.1074/jbc.M506056200 PMID: 16150697

56. Zhang K, Myllymäki SM, Gao P, Devarajan R, Kytölä V, Nykter M, et al. Oncogenic K-Ras upregulates ITGA6 expression via FOSL1 to induce anoikis resistance and synergizes with αV-Class integrins to promote EMT. Oncogene. 2017; 36:5681–94. https://doi.org/10.1038/onc.2017.177 PMID: 28604746

57. Liu Y, Yue M, Li Z. FOSL1 promotes tumorigenesis in colorectal carcinoma by mediating the FBXL2/Wnt/β-catenin axis via Smurf1. Pharmacol Res. 2021; 165:105495. https://doi.org/10.1016/j.phrs.2020.105405 PMID: 33450386

58. Leong GM, Subramaniam N, Figueroa J, Flanagan JL, Hayman MJ, Eisman JA, et al. Ski-interacting protein interacts with Smad proteins to augment transforming growth factor-beta-dependent transcription. J Biol Chem. 2001; 276:18243–8 https://doi.org/10.1074/jbc.M010815200 PMID: 11278756

59. Wang Y, Fu Y, Gao L, Zhu G, Liang J, Gao C, et al. Xenopus skip modulates Wnt/beta-catenin signaling and functions in neural crest induction. J Biol Chem 2010; 285:10890–901. https://doi.org/10.1074/jbc.M109.058347 PMID: 20103590

60. Filla MS, Meyers KA, Faralli JA, Peters DM. Overexpression and activation of αvβ3 integrin differentially affects TGFβ2 signaling in human trabecular meshwork cells. Cells. 2021; 10:1923. https://doi.org/10.3390/cells10081923 PMID: 34440692

61. Tsujimoto G, Ito R, Yoshikawa K, Ueki C, Okada N. NFYA promotes the anti-tumor effects of gluconeogenesis in hepatocellular carcinoma through the regulation of PCK1 expression. Front Cell Dev Biol. 2022; 10:983599. https://doi.org/10.3389/fcell.2022.983599 PMID: 36092708

62. Simpson TI, Price DJ. Pax6; a pleiotropic playerin development. BioEssays. 2002; 24:983–1081. https://doi.org/10.1002/bies.10174 PMID: 12386935

63. Ohira T, Kojima H, Kuroda Y, Aoki S, Inaoka D, Osaki M, et al. PITX1 protein interacts with ZCCHC10 to regulate hTERT mRNA transcription. PLoS One. 2019; 14:e0217605. https://doi.org/10.1371/journal.pone.0217605 PMID: 31404068

64. Kolfschoten IGM, van Leeuwen B, Berns K, Mullenders J, Beijersbergen RL, Bernards R, et al. A genetic screen identifies PITX1 as a suppressor of RAS activity and tumorigenicity. Cell. 2005; 17:849–58. https://doi.org/10.1016/j.cell.2005.04.017 PMID: 15960973

65. Sobolev VV, Khashukoeva AZ, Evina OE, Geppe NA, Chebysheva SN, Korsunskaya IM, et al. Role of the transcription factor FOSL1 in organ development and tumorigenesis. Int J Mol Sci. 2022; 23:1521. https://doi.org/10.3390/ijms23031521 PMID: 35163444

66. Roth L, Srivastava S, Lindzen M, Sas-Chen A, Sheffer M, Lauriola M, et al. SILAC identifies LAD1 as a filamin-binding regulator of actin dynamics in response to EGF and a marker of aggressive breast tumors. Sci Signal. 2018; 11:eaan0949. https://doi.org/10.1126/scisignal.aan0949 PMID: 29382783

67. Keller KE, Bradley JM, Vranka JA, Acott TS. Segmental versican expression in the trabecular meshwork and involvement in outflow facility. Invest Ophthamol Vis Sci. 2011; 52:5049–57. https://doi.org/10.1167/iovs.10-6948 PMID: 21596823

68. Hill LJ, Mead B, Blanch RJ, Ahmed Z, De Cogan F, Morgan-Warren PJ, et al. Decorin reduces intraocular pressure and retinal ganglion cell loss in rodents through fibrolysis of the scarred trabecular meshwork. Invest Ophthalmol Vis Sci. 2015; 56:3743–57. https://doi.org/10.1167/iovs.14-15622 PMID: 26066743

69. Faralli JA, Filla MS, Peters DM. Effect of αvβ3 integrin expression and activity on intraocular pressure (IOP). Invest Ophthalmol Vis Sci. 2019; 60:1776–88. https://doi.org/10.1167/iovs.18-26038 PMID: 31022732

70. Acott TS, Kelley MJ, Keller KE, Vranka JA, Abu-Hassan DW, Li X, et al. Intraocular pressure homeostasis: Maintaining balance in a high-pressure environment. J Occul Pharmacol. 2014; 30:94–101. https://doi.org/10.1089/jop.2013.0185 PMID: 24401029

71. Yang Y-F, Sun YY, Peters DM, Keller KE. The effects of mechanical stretch on integrins and filopodial-associated proteins in normal and glaucomatous trabecular meshwork cells. Front Cell Dev Biol. 2022; 10:886706. https://doi.org/10.3389/fcell.2022.886706 PMID: 35573666

72. Böhm BB, Aigner T, Roy B, Brodie TA, Blobel CP, Burkhardt H. Homeostatic effects of the metalloproteinase disintegrin ADAM15 in degenerative cartilage remodeling. Arthritis Rheumat. 2005; 52:1100–9. https://doi.org/10.1002/art.20974 PMID: 15818704

73. Jana S, Chute M, Hu M, Winkelaar G, Owen CA, Oudit GY, et al. ADAM (a Disintegrin and Metalloproteinase) 15 deficiency exacerbates Ang II (Angiotensin II)–induced aortic remodeling leading to abdominal aortic aneurysm. Arterioscler Thromb Vasc Biol. 2020; 40:1918–34. https://doi.org/10.1161/ATVBAHA.120.314600 PMID: 32522006

74. Chute M, Aujla PK, Li Y, Jana S, Zhabyeyev P, Rasmuson J, et al. ADAM15 is required for optimal collagen cross-linking and scar formation following myocardial infarction. Matrix Biol. 2022; 105:127–43. https://doi.org/10.1016/j.matbio.2021.12.002 PMID: 34995785

75. Janczi T, Meier F, Fehrl Y, Kinne RW, Bohm B, Burkhardt H. A novel pro-inflammatory mechanosensing pathway orchestrated by the disintegrin metalloproteinase ADAM15 in synovial fibroblasts. Cells. 2021; 10:2705. https://doi.org/10.3390/cells10102705 PMID: 34685689

76. Calligaris M, Yang CY, Bonelli S, Spanò DP, Müller SA, Lichtenthaler SF, et al. Identification of membrane proteins regulated by ADAM15 by SUSPECS proteomics. Front Mol Biosci. 2023; 10:1162504. https://doi.org/10.3389/fmolb.2023.1162504 PMID: 37388246

77. Park M, Ohana E, Choi SY, Lee M-S, Park JH, Muallem S. Multiple roles of the SO4 2/Cl/OH exchanger protein Slc26a2 in chondrocyte functions. J Biol Chem. 2014; 289:1993–2001. https://doi.org/10.1074/jbc.M113.503466 PMID: 24302720

78. Acott TS, Westcott M, Passo MS, Van Buskirk EM. Trabecular meshwork glycosaminoglycans in human and cynomolgus monkey eye. Invest Ophthalmol Vis Sci. 1985; 26:1320–9. PMID: 4044160

79. Knepper PA, Goossens W, Hvizd M, Palmberg PF. Glycosaminoglycans of the human trabecular meshwork in primary open-angle glaucoma. Invest Ophthalmol Vis Sci. 1996; 37:1360–7. PMID: 8641839

80. Adhikari B, Osmond MJ, Pantcheva MB, Krebs MD. Glycosaminoglycans influence extracellular matrix of human trabecular meshwork cells cultured on 3D scaffolds. ACS Biomater Sci Eng. 2020; 8:5221–32. https://doi.org/10.1021/ascbiomaterials.2c00457

81. Vogel S, Anrnoldini S, Moller S, Schnabelrauch M, Hempel U. Sulfated hyaluronan alters fibronectin matrix assembly and promotes osteogenic differentiation of human bone marrow stromal cells. Sci Rep. 2016; 6:36418. https://doi.org/10.1038/srep36418 PMID: 27808176

82. Soares da Costa D, Reis RL, Pashkuleva I. Sulfation of glycosaminoglycans and its implications in human health and disorders Annu Rev Biomed Eng 2017; 19:1–26. https://doi.org/10.1146/annurev-bioeng-071516-044610 PMID: 28226217

83. Eto K, Puzon-McLaughlin W, Sheppard D, Sehara-Fujisawa A, Zhang X-P, Takada Y. RGD-independent binding of integrin α9β1 to the ADAM-12 and -15 disintegrin domains mediates cell-cell interaction. J Biol Chem. 2000; 275:34922–330. https://doi.org/10.1074/jbc.M001953200 PMID: 10944520

84. Nath D, Slocombe P, Stephens P, Warn A, Hutchinson G, Yamada KM, et al. Interaction of metargidin (ADAM-15) with alphavbeta3 and alpha5beta1 integrins on different haemopoietic cells. J Cell Sci 1999; 112 579–87. https://doi.org/10.1242/jcs.112.4.579 PMID: 9914169

85. Zhou J, Wang A, Cai T, Li Y, Du W, Zhang Y, et al. Integrin α3/α6 and αV are implicated in ADAM15-activated FAK and EGFR signalling pathway individually and promote non-small-cell lung cancer progression. Cell Death Dis. 2022; 13:486. https://doi.org/10.1038/s41419-022-04928-0 PMID: 35597804

86. Aujla PK, Hu M, Hartley B, Kranrod JW, Viveiros A, Kilic T, et al. Loss of ADAM15 exacerbates transition to decompensated myocardial hypertrophy and dilation through activation of the calcineurin pathway. Hypertension. 2023; 80:97–110. https://doi.org/10.1161/HYPERTENSIONAHA.122.19411 PMID: 36330793

87. Babendreyera A, Mollsa L, Simonsa IM, Dreymuellera D, Billera K, Jahr H, et al. The metalloproteinase ADAM15 is upregulated by shear stress and promotes survival of endothelial cells. J Mol Cell Cardiol. 2019; 134:51–61. https://doi.org/10.1016/j.yjmcc.2019.06.017 PMID: 31271758

88. Mao M, Hedberg-Buenz A, Koehn D, John SWM, Anderson MG. Anterior Segment Dysgenesis and Early-Onset Glaucoma in nee Mice with Mutation of Sh3pxd2b. Invest Ophthamol Vis Sci. 2011; 52:2679–88. https://doi.org/10.1167/iovs.10-5993 PMID: 21282566

89. Mao M, Thedens DR, Chang B, Harris BS, Zheng QY, Johnson KR, et al. The podosomal-adaptor protein SH3PXD2B is essential for normal postnatal development Mamm Genome. 2009; 20:462–75. https://doi.org/10.1007/s00335-009-9210-9 PMID: 19669234

90. Aga M, Bradley JM, Keller KE, Kelley MJ, Acott TS. Specialized podosome- or invadopodia-like structures (PILS) for focal trabecular meshwork extracellular matrix turnover. Invest Ophthalmol Vis Sci. 2008; 49:5353–65. https://doi.org/10.1167/iovs.07-1666 PMID: 18641286

91. Keller KE, Bradley JM, Acott TS. Differential effects of ADAMTS-1, -4, and -5 in the trabecular meshwork. Invest Ophthalmol Vis Sci. 2009; 50:5769–77. https://doi.org/10.1167/iovs.09-3673 PMID: 19553617

92. Osmond MJ, Krebs MD, Pantcheva MB. Human trabecular meshwork cell behavior is influences by collagen scaffold pore architecture and glycosaminoglycan composition. Biotechnol Bioeng. 2019; 117:3150–9. https://doi.org/10.1002/bit.27477 PMID: 32589791

93. Doyle MD, Carvajal N, Jin A, Matsumoto K, Yamada KM. Local 3D matix microenvironment regulates cell migration through spatiotemporal dynamics of cell contractility-dependent adhesions. Nat Commun. 2015; 6:8720. https://doi.org/10.1038/ncomms9720 PMID: 26548801

94. Xie J, Bao M, Bruekers SMC, Huck WTS. Collagen gels with different fibrillar microarchitectures elicit different cellular responses. ACS Appl Mater Interfaces. 2017; 9:19630–7. https://doi.org/10.1021/acsami.7b03883 PMID: 28537381

95. Kitchen CM, Cowan SL, Long X, Miano JM. Expression and promoter analysis of a highly restricted integrin alpha gene in vascular smooth muscle. Gene. 2013; 513:82–9. https://doi.org/10.1016/j.gene.2012.10.073 PMID: 23142384

96. Marek I, Hilgers KF, Rascher W, Woelfle J, Hartner A. A role for the alpha-8 integrin chain (itga8) in glomerular homeostasis of the kidney. Mol Cell Pediatr. 2020; 7:13. https://doi.org/10.1186/s40348-020-00105-5 PMID: 33000355

97. Marek I, Volkert G, Jahn A, Fahlbusch F, Zürn C, Ozcan Z, et al. Lack of α8 integrin leads to morphological changes in renal mesangial cells, but not in vascular smooth muscle cells. BMC Cell Biol. 2010; 11:102. https://doi.org/10.1186/1471-2121-11-102 PMID: 21194485

98. Zargham R, Touyz RM, Thibault G. Alpha 8 integrin overexpression in de-differentiated vascular smooth muscle cells attenuates migratory activity and restores the characteristics of the differentiated phenotype. Atherosclerosis. 2007; 195:303–12. https://doi.org/10.1016/j.atherosclerosis.2007.01.005 PMID: 17275006

99. Ma J, Bi L, Spurlin J, Lwigale P. Nephronectin-integrin α8 signaling is required for proper migration of periocular neural crest cells during chick corneal development. eLife. 2022; 11:e74307. https://doi.org/10.7554/eLife.74307 PMID: 35238772